RAPID COMMUNICATIONS

PHYSICAL REVIEW E VOLUME 53, NUMBER 4 APRIL 1996

Amplitude, wave form, and temperature dependence of bilayer ripples in the $P_{\beta'}$ phase

J. T. Woodward IV
Department of Physics, University of California, Santa Barbara, California 93106-5080

J. A. Zasadzinski*
Department of Chemical Engineering, University of California, Santa Barbara, California 93106-5080
(Received 12 July 1995)

Scanning tunneling microscopy–freeze-fracture replication has provided a quantitative, high resolution description of the wave form and amplitude of rippled bilayers in the $P_{\beta'}$ phase of dimyristoylphosphatidylcholine. The ripples are uniaxial and asymmetric, with a temperature dependent amplitude of 2.4 nm near the chain melting temperature decreasing to zero at the chain crystallization temperature. The wavelength of 11 nm does not change with temperature. The observed ripple shape and the temperature induced structural changes are not predicted by any current theory.

PACS number(s): 87.15.Da, 87.64.Dz, 87.80.+s

The self-assembly and phase behavior of phospholipids in water have been studied extensively as simple biophysical models of the cell membrane [1]. Morphological changes often accompany phase changes in lipid-water bilayers, making them of physical interest as examples of transitions in nearly two-dimensional systems [2–21]. In particular, bilayers of saturated phosphatidylcholines undergo three distinct structural transitions when dispersed in water: a subtransition, a pretransition, and a main transition separating the phases L_c, $L_{\beta'}$, $P_{\beta'}$, and L_α [2–5]. In the high temperature L_α phase, the order within each bilayer is short range and the *trans-gauche* intramolecular order is low [2–8]. The main transition is associated with lipid chain melting [2–7]. The bilayers are smooth and the molecules, on average, are normal to the bilayer [2–6]. The $L_{\beta'}$ phase is characterized by flat bilayers with the lipid chains fully extended (all-*trans* configuration) and tilted with respect to the bilayer normal. The positional order appears to be short range and the orientational order longer ranged [5]. The magnitude and direction of tilt depends on the water fraction [5]. The low temperature $L_{\beta'} \rightarrow L_c$ transition involves a modification of the chain packing and dehydration of the head groups [3]. Elucidating the structure of lipid bilayers has taken on an additional significance in the light of recent experiments that have shown that the lipid membrane is more than a passive matrix for biologically active proteins [1]; protein function can be modified by the composition, phase and local structure of the lipids [22,23].

A satisfactory explanation of the $P_{\beta'}$ or ripple phase remains a challenge primarily because of the lack of quantitative information on the ripple structure. It is known that in the $P_{\beta'}$ phase, the lipid chains retain much of their all-*trans* configuration [2–7], and the molecules are packed into a two-dimensional hexagonal lattice with long-range orientational order [2–12]. The bilayers are characterized by regular three-dimensional corrugations, hence the common name of ripple phase. X-ray diffraction and freeze-fracture electron microscopy find the ripple wavelength in excess water to be about 10–15 nm [2–11]. The ripples in the $P_{\beta'}$ phase are capable of aligning large molecules such as proteins along their length; diffusion within the plane of the bilayer appears to be anisotropic [24]. Replacing one or more methyl groups from the choline headgroup by hydrogen, thereby decreasing the size of the headgroup relative to the chains, eliminates the $P_{\beta'}$ phase [10]. Models of the $P_{\beta'}$ phase fall into two broad classes: phenomenological models based on modulations of membrane thickness [13–16] or curvature [17,18] and molecular models based on packing frustration between the lipid headgroup and chains [19–21]. Many physical models can find a sinusoidal minimum energy configuration; to distinguish between these theories requires that the amplitude, wave form, and wavelength of the ripples be measured with high resolution. Unfortunately, the ripple shape cannot be determined by x-ray diffraction or by conventional freeze-fracture electron microscopy. However, using a refined freeze-fracture–scanning tunneling microscopy (STM) technique we have developed [12,26,28], it is possible to quantitatively determine the three-dimensional shape and temperature dependence of $P_{\beta'}$ bilayers to show that current models of the ripple phase [14–21] are insufficient.

Metal replicas of dimyristoylphosphatidylcholine (DMPC) bilayers at full hydration equilibrated at 16, 18, 20 and 23 °C were prepared for both TEM and STM to determine the temperature dependence of the ripple amplitude, wave form, and wavelength (the $P_{\beta'}$ phase of DMPC exists from 14–24 °C). For each sample, 200 mg of DMPC (Avanti Polar Lipids, Atlanta, Georgia) was added to 0.2 ml Milli-Q water (Millipore, Bedford, MA); the resulting 50% DMPC–50% water mixture ensured that the bilayers are fully hydrated [2–5]. The samples were alternately centrifuged at low speed, vortexed, then heated at >30 °C for at least 24 h to allow complete mixing. Thin films of the DMPC-water mixture were sandwiched between copper freeze-fracture planchettes, then equilibrated at 100% relative humidity at 23, 20, 18, or 16 °C prior to rapid quenching in liquid propane cooled by liquid nitrogen [26]. Freeze-fracture replication was done in a Balzers 400 freeze-etch machine [26–28]. The TEM samples were shadowed with 1.5 nm of Pt-C at a

*Author to whom correspondence should be addressed. FAX: 805-893-4731. Electronic address: gorilla@squid.ucsb.edu

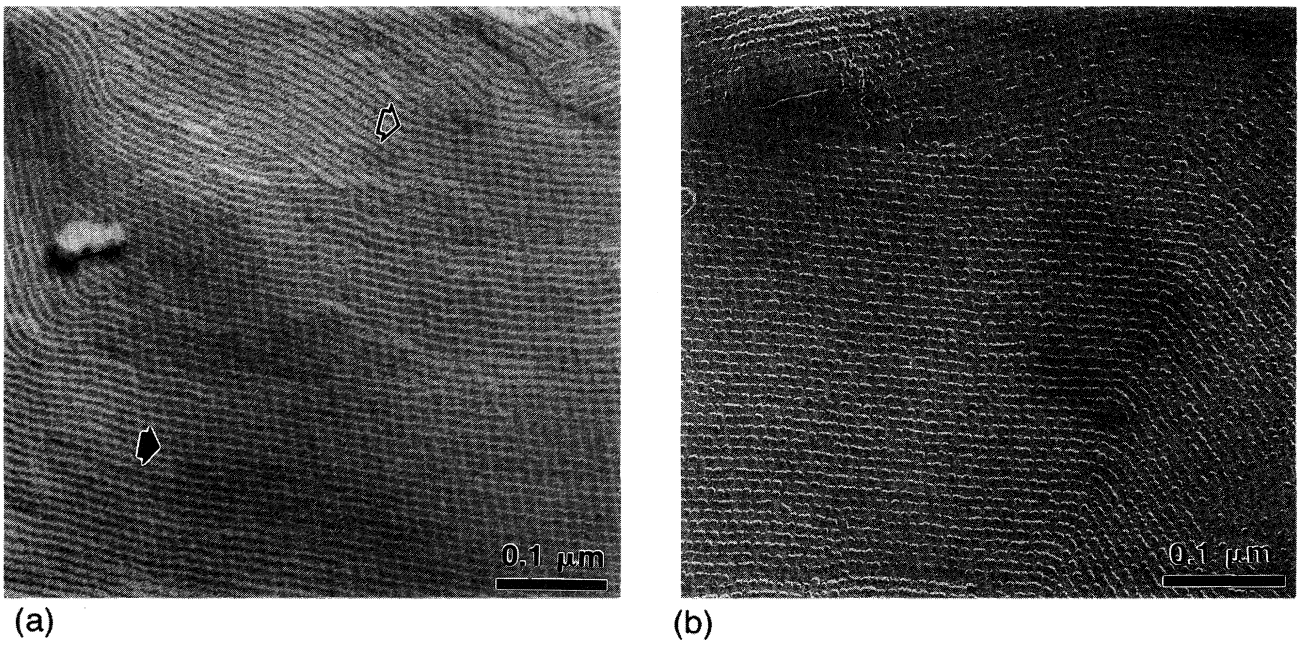

FIG. 1. (a) TEM image of DMPC in excess water at 23 °C. The ripples change orientation over micrometer length scales, typically at 120° angles, indicating an underlying hexagonal packing. The ripple asymmetry can be inferred from the shadow patterns—narrow, dark gray—wide, light gray lines in the upper left of the image (open arrow) adjacent to narrow, white—wide, dark gray lines in the lower right of the image (filled arrow) [10]. (b) TEM image of DMPC in excess water at 16 °C (The sample at 18 °C was similar). The ripples are much less well defined and appear like a string of beads. This beading is induced by a self-shadowing process that enhances small features [31]. The ripple amplitude is much smaller and the asymmetry in the shadowing has disappeared.

45° angle relative to the surface, while the STM samples were coated normal to the surface. A 15 nm thick film of carbon was added to stabilize the shadowing film. In previous experiments [12], we did not appreciate that capillary condensation from lab air could couple the STM tip to the metal replica and lead to an artificial amplification of the feature heights [27,28]. To eliminate the amplification, replicas for STM had an additional 0.5 micrometer thick layer of silver deposited by sputtering to increase film rigidity. STM [25] (Digital Instruments, Santa Barbara, CA) imaging was done under a dry nitrogen atmosphere to further eliminate the possibility of condensation [26–28]. Each sample was examined with several different cut Pt-Ir tips with a 12 μm scanning head in the constant current mode. The vertical piezo of the STM was calibrated with replicas of cadmium arachidate Langmuir-Blodgett films [27] of known step heights [29].

Representative TEM images of the 23 °C and 16 °C samples are shown in Fig. 1. In the 23 °C and 20 °C samples, the ripples are continuous and the ripple asymmetry is apparent from the variation in shadowing across the image [Fig. 1(a)] [10]. In TEM images of the 18 °C and 16 °C samples,

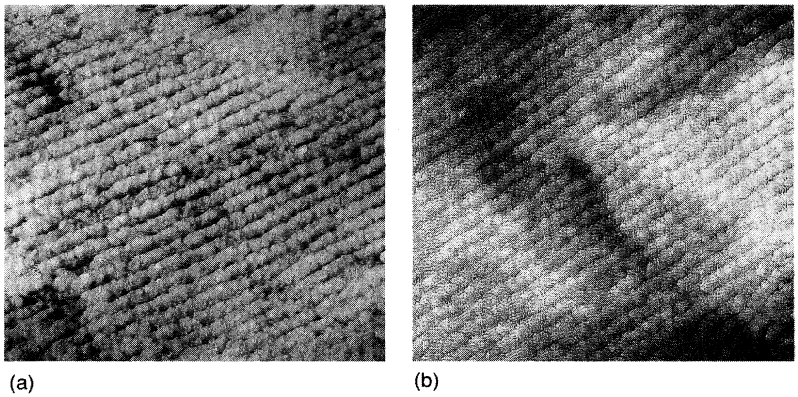

FIG. 2. (a) 250 nm×250 nm STM image of a freeze-fracture replica of DMPC in excess water originally at 23 °C. The ripple shape is obscured by the finite size of the metal grains that make up the replica film, imperfections in the ripples themselves, and noise from the STM. Correlation averaging helps eliminate these features to enhance the image quality. (b) 250 nm×250 nm STM image of a freeze-fracture replica of DMPC in excess water originally at 20 °C. The apparent amplitude of the ripples has decreased as compared with (a).

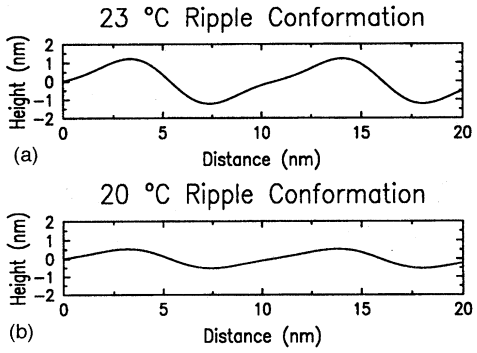

FIG. 3. (a) Average ripple cross section at 23 °C as determined from the average of the parameters from the correlation averaging. The wavelength is 10.7±1 nm and the peak to valley amplitude is 2.4 nm. (b) Average ripple cross section at 20 °C. The wavelength is 10.6±1 nm and the peak to valley height decreases to 1.1 nm. The asymmetry in the wave form is still present.

the ripples are discontinuous and appear to be made up of a line of beads. This pattern of beads is consistent with a self-shadowing artifact; the oblique metal deposition enhances small features in the fracture surface [31]. It is clear that the ripple is of smaller amplitude, and that the shadowing pattern has lost its asymmetry and is less well defined, suggesting a temperature dependence of the ripple amplitude. When the replica is made by depositing the metal film normal to the surface (which eliminates self-shadowing), TEM images of the 18 °C and 16 °C samples are featureless. The wavelength of the ripples is 11.0±1.0 nm for all four temperatures. The measured values for the wavelength are in good agreement with the value of 11–12 nm found by x-ray diffraction [3,4] or freeze-fracture TEM of DMPC [8–11].

250×250 nm STM images with the ripples oriented in a single direction were analyzed to quantify the ripple features observed by TEM. At this image size, each ripple has about 20 pixels per wavelength (images are 512×512 pixels). Figure 2 shows representative images from the 23 °C and the 20 °C samples. Samples prepared at 18 °C and 16 °C showed no modulated textures. Lower resolution STM scans of both the 23 °C and the 20 °C samples show that the STM and TEM images have the same defect patterns and general features [28]. Fourier transforms of both the smaller and larger scale images were used to evaluate the ripple wavelength, which was consistent with the TEM results. STM images suitable for analysis were averaged using a structure function program [28,30] on a Silicon Graphics Indigo computer. The averaging program works by taking a small test area of the image and cross-correlating the test area with the entire image. A test area size of 32×32 pixels was used to ensure that the test area contained at least one complete ripple. Areas that showed a minimum square deviation from the test image were then averaged to make a composite image [30]. The composite image was then used as the test image to determine a new composite and eliminate any bias in the original choice of test image. Typically 1000–4000 areas were used to make a composite [28].

The average ripple conformation determined from the composite image was then fit to a sum of harmonics using the nonlinear least squares fitting routine found in C-PLOT

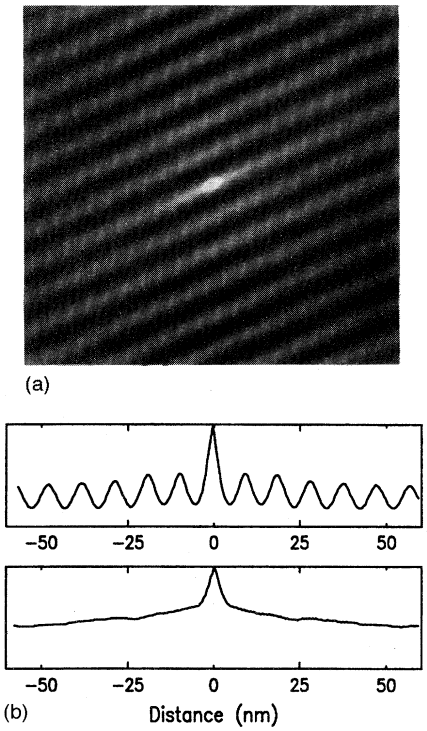

FIG. 4. (a) Autocorrelation of the sample quenched from 23 °C shown in Fig. 2(a). (b) Cross sections of (a) along (top) the ripple direction and (bottom) perpendicular to the ripple direction. The lack of modulation perpendicular to the ripple direction rules out any significant secondary modulation [12].

(Cambridge, MA) to eliminate any systematic errors introduced by specific samples, images, STM tips, etc. The parameters fit were the amplitudes and phases of the first three harmonics of a sine wave, and the wavelength of the ripple. The average values of the first two harmonics for the 23 °C samples are 1.1±0.3 nm and 0.3±0.1 nm, and the averaged wavelength is 10.7±1.0 nm. For the 20 °C samples, the amplitude of the first harmonic is 0.5±0.2 nm, the second amplitude is 0.1±0.1 nm, and the wavelength is 10.6±1.0 nm. The amplitude of the third harmonic was negligible for both temperatures. Figure 3 shows a cross section of the ripple conformation calculated from the average values. The fits give a peak to valley height of 2.4 nm for the ripple at 23 °C and 1.1 nm at 20 °C. Combined with the zero amplitude [32] we found at 18 °C and 16 °C, this shows a distinct temperature dependence of the ripple amplitude in the $P_{\beta'}$ phase. Our previous estimate of the ripple peak to valley height was 4.5 nm, based on a very limited number of STM images taken in air [12]. This peak to valley height was undoubtedly amplified by the coupling between the STM tip and the replica in these preliminary experiments [27]. Both STM and TEM measurements show that the ripple wavelength of 11±1 nm is invariant with temperature. This is consistent with the results of Matuoka *et al.*, who found that the ripple wavelength of pure DMPC changed very little over the temperature range of 16–24 °C [33].

In addition to an artificially large amplitude, the filtered images of our earlier experiments showed a small secondary

ripple perpendicular to the primary ripple [12]. X-ray results have suggested that this secondary ripple may be due to molecular tilt perpendicular to the ripple wave vector [6]. However, Fourier transforms of our STM and TEM images do not have any peaks other than those of the primary ripple. As a check for the secondary ripple we looked at autocorrelations of the STM images and found no periodicity perpendicular to the primary ripple. Figure 4 shows the autocorrelation and cross sections from the image shown in Fig. 2(a).

Bilayers of DMPC in excess water have uniaxial, asymmetric ripples that decrease from 2.4 nm peak to peak near the chain melting temperature to near zero near the chain crystallization temperature. The ripple wavelength of 11 nm does not change with temperature. The magnitude of the ripple amplitude we have measured is too large to be consistent with variations in membrane thickness due to localized melting as suggested by Goldstein and Liebler [15]. The asymmetric ripple shape is consistent with a recent theory that suggests the ripple is the result of a coupling between molecular tilt and bilayer bending [18]. However, in this theory, the asymmetric ripple requires a chiral packing that is inconsistent with experimental observations [7,11]. Most importantly, the temperature dependence of the ripple amplitude has not to our knowledge previously been observed experimentally nor been predicted theoretically. However, it can be rationalized, as the bend elasticity of the membrane should decrease dramatically over the transition from crystalline to fluid bilayers as the temperature is raised through the $P_{\beta'}$ phase. The softening bilayer would be expected to buckle with a greater amplitude. Both STM and TEM show that the wavelength of the ripples is unchanged at all four temperatures. This indicates that models of the ripple phase based on a fixed offset of neighboring molecules due to packing frustration must be modified [19]. Such theories predict that the wavelength of the ripple would scale with the amplitude, in contradiction to our results. However, a change in molecular tilt with temperature might change the vertical component of a fixed molecular offset as the temperature increases from the tilted $L_{\beta'}$ phase to the untilted L_{α} phase. We have also carefully investigated the possibility of a second ripple normal to the first set of ripples by examining autocorrelations of the ripple images. No secondary ripple structure was found, indicating that previous indications of such ripples were likely artifacts [12] and they are not related to a change in hydrocarbon tilt direction [6].

We thank R. Viswanathan for preparing Langmuir-Blodgett films and L. Madsen for help with correlation averaging. This work was supported by NIH Grant No. HL51177, and made use of MRL Central Facilities under NSF No. DMR-9123048.

[1] S. J. Singer and G. L. Nicolson, Science **175**, 720 (1972).
[2] A. Tardieu, V. Luzzati, and F. C. Reman, J. Mol. Biol. **75**, 711 (1973).
[3] M. J. Janiak, D. M. Small, and G. G. Shipley, J. Biol. Chem. **254**, 6068 (1979).
[4] D. C. Wack and W. W. Webb, Phys. Rev. Lett. **61**, 1210 (1988); Phys. Rev. A **40**, 2712 (1989).
[5] E. B. Sirota *et al.*, Science **242**, 1406 (1988); G. S. Smith *et al.*, Mol. Cryst. Liq. Cryst. **144**, 235 (1987).
[6] M. P. Hentschel and F. Rustichelli, Phys. Rev. Lett. **66**, 903 (1991).
[7] J. Katsaras and V. A. Raghunathan, Phys. Rev. Lett. **74**, 2022 (1995).
[8] E. J. Luna and H. M. McConnell, Biochim. Biophys. Acta **466**, 381 (1977).
[9] D. Ruppel and E. Sackmann, J. Phys. (Paris) **44**, 1025 (1983).
[10] J. A. Zasadzinski and M. B. Schneider, J. Phys. (Paris) **48**, 2001 (1987).
[11] J. A. Zasadzinski, Biochim. Biophys. Acta **946**, 235 (1988).
[12] J. A. Zasadzinski *et al.*, Science **239**, 1013 (1988).
[13] C. Gephardt, H. Gruler, and E. Sackmann, Z. Naturforsch Teil C **32**, 581 (1977).
[14] M. Marder *et al.*, Proc. Natl. Acad. Sci. USA **81**, 6559 (1984).
[15] R. E. Goldstein and S. Liebler, Phys. Rev. Lett. **61**, 2213 (1988).
[16] G. Cevc, Biochim. Biophys. Acta **1062**, 59 (1991).
[17] S. Doniach, J. Chem. Phys. **70**, 4587 (1979).
[18] T. C. Lubensky and F. C. MacKintosh, Phys. Rev. Lett. **71**, 1565 (1993).
[19] H. L. Scott and W. S. McCullough, Phys. Rev. Lett. **65**, 931 (1990).
[20] J. M. Carlson and J. P. Sethna, Phys. Rev. A **36**, 3359 (1987).
[21] D. K. Schwartz, R. Viswanathan, and J. A. Zasadzinski, J. Chem. Phys. **101**, 7161 (1994).
[22] S. L. Keller *et al.*, Biophys. J. **65**, 23 (1993).
[23] M. L. Longo *et al.*, Science **261**, 453 (1993).
[24] M. B. Schneider, W. K. Chan, and W. W. Webb, Biophys. J. **43**, 157 (1983).
[25] G. Binnig *et al.*, Phys. Rev. Lett. **49**, 57 (1982).
[26] J. A. Zasadzinski and S. M. Bailey, J. Elect. Microsc. Tech. **13**, 309 (1989); J. R. Bellare *et al.*, *ibid.* **10**, 87 (1988).
[27] J. T. Woodward and J. A. Zasadzinski, Langmuir **10**, 1340 (1994).
[28] J. T. Woodward, Ph.D. thesis, University of California, Santa Barbara, 1994 (unpublished).
[29] J. A. Zasadzinski *et al.*, Science **263**, 1726 (1994).
[30] J. T. Woodward *et al.*, J. Microscopy (Oxford) **178**, 86 (1995).
[31] G. Ruben, J. Electron Microsc. Tech. **13**, 335 (1989).
[32] The minimum vertical ripple height that can be resolved with this technique is about 0.3–0.5 nm. Hence, for the 18 °C and 16 °C samples, we can be confident that the ripple is less than this minimum value.
[33] S. Matuoka, S. Kato, and I. Hatta, Biophys. J. **67**, 728 (1994); K. Mortensen *et al.*, Biochim. Biophys. Acta **945**, 221 (1988).

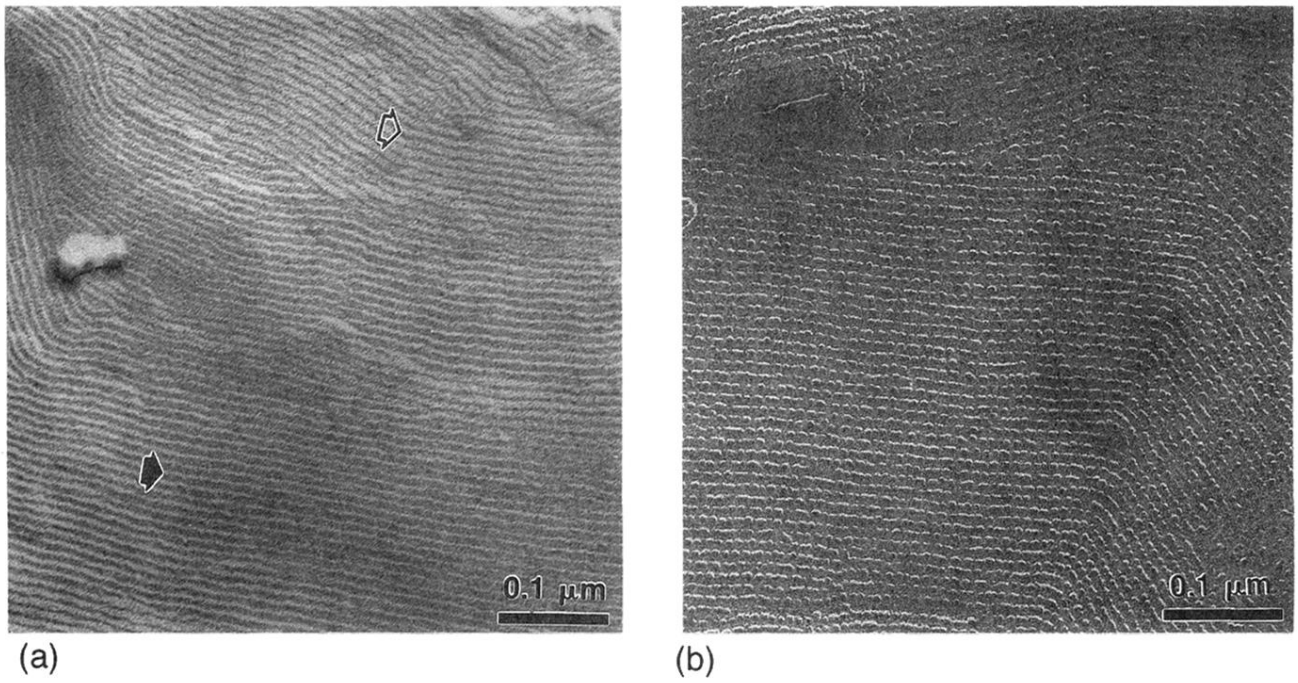

FIG. 1. (a) TEM image of DMPC in excess water at 23 °C. The ripples change orientation over micrometer length scales, typically at 120° angles, indicating an underlying hexagonal packing. The ripple asymmetry can be inferred from the shadow patterns—narrow, dark gray—wide, light gray lines in the upper left of the image (open arrow) adjacent to narrow, white—wide, dark gray lines in the lower right of the image (filled arrow) [10]. (b) TEM image of DMPC in excess water at 16 °C (The sample at 18 °C was similar). The ripples are much less well defined and appear like a string of beads. This beading is induced by a self-shadowing process that enhances small features [31]. The ripple amplitude is much smaller and the asymmetry in the shadowing has disappeared.

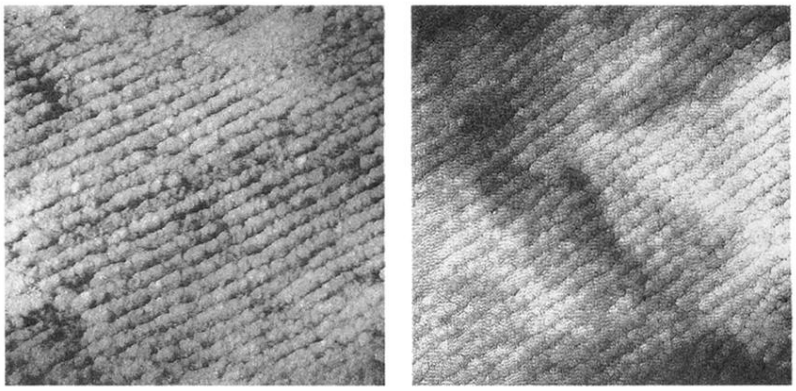

FIG. 2. (a) 250 nm×250 nm STM image of a freeze-fracture replica of DMPC in excess water originally at 23 °C. The ripple shape is obscured by the finite size of the metal grains that make up the replica film, imperfections in the ripples themselves, and noise from the STM. Correlation averaging helps eliminate these features to enhance the image quality. (b) 250 nm×250 nm STM image of a freeze-fracture replica of DMPC in excess water originally at 20 °C. The apparent amplitude of the ripples has decreased as compared with (a).

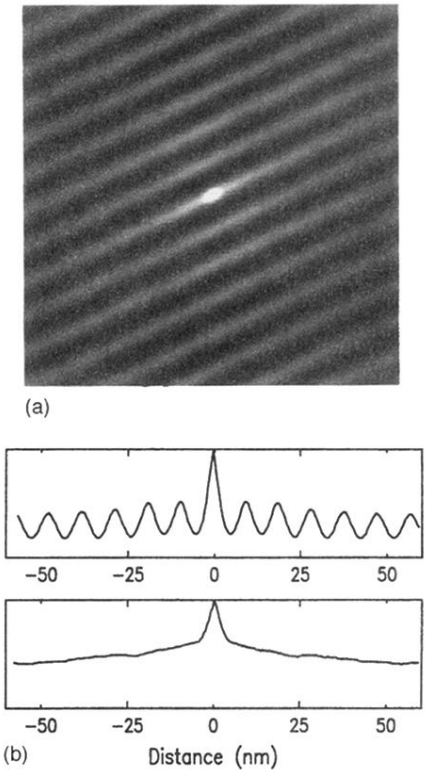

FIG. 4. (a) Autocorrelation of the sample quenched from 23 °C shown in Fig. 2(a). (b) Cross sections of (a) along (top) the ripple direction and (bottom) perpendicular to the ripple direction. The lack of modulation perpendicular to the ripple direction rules out any significant secondary modulation [12].